# 5 2D or not 2D

## Reduced ion migration by addition of a 2D layer, comparing PEA, FEA and mixed PEA/FEA

2D/3D perovskite solar cells, where a thin 2D perovskite layer is deposited onto a thick 3D perovskite layer, have recently emerged as a promising avenue to combine both the high efficiency of the 3D perovskites and the increased stability of the 2D perovskites. In fully 2D perovskite devices, ion migration appears to be reduced or suppressed compared to the fully 3D systems. However, it remains unclear if ion migration in a 2D/3D perovskite solar cell is affected by the presence of the thin 2D layer at the interface between the 3D perovskite and the hole transport layer. Here, we study the influence of the addition of this thin 2D layer on ion migration in the full 2D/3D solar cell devices. We further evaluate the effect of the 2D spacer layer composition by varying the 2D spacer molecules between FEA, PEA or a mix of FEA and PEA, and find that in all devices incorporating a 2D layer, ion migration is hindered. Upon addition of the FEA 2D layer, the density of one of the mobile halide ions decreases from 41 % to 15 % of the doping density; while addition of the PEA 2D layer affects the second mobile halide ion, by decreasing its density from 60 % to 25 % of the doping density, and increasing the migration activation energy from 65 meV to 110 meV. Our quantitative analysis of ion migration thus allows us to distinguish different mechanisms of ion migration suppression, dependent on the 2D spacer composition.

This chapter is based on the following publication:
Lucie McGovern, Rens van Roosmalen, Anwar Alanazi, Gianluca Grimaldi, Moritz C. Schmidt, Jovana V. Milić and Bruno Ehrler, "Effect of a 2D layer on ion migration in perovskite solar cells, comparing PEA, FEA and mixed PEA/FEA systems", in preparation.

## 5.1 Introduction

Perovskite solar cells have recently emerged as one of the most promising material platforms for optoelectronic devices. Combining high Power Conversion Efficiencies (PCEs)[159–161], cheap synthesis and fabrication methods[162–164], and bandgap tunability by simple modification of the perovskite composition[11], they appear as an outstanding candidate in the field of photovoltaic research[10], where efforts for better and cheaper solar cells are continuously ongoing. However, perovskite solar cells are still affected by a major drawback, which is their instability. Modules tend to degrade with time and have been shown to be sensitive to a range of environmental factors[19,165,166], impeding their large-scale commercialisation. Ion migration, the process whereby an ion from the $ABX_3$ perovskite structure detaches and becomes mobile within the perovskite layer, is a particular challenge in lead halide perovskites, as it is an intrinsic source of instability in these devices[60]. Finding a reliable, simple, and robust mitigation strategy against ion migration in perovskite solar cells is thus a desirable goal, which would allow these devices to contribute to the ever-growing global need for energy[167].

In this context, 2D perovskite devices have recently emerged as an opportunity for increased stability in the field of perovskite solar cells[168–171]. In 2D perovskite layers, the lead halide inorganic sheets are separated by organic spacer molecules (called 2D spacer molecules), which are large organic cations that replace some of the small A-site cations present in the 3D perovskites[169]. The general formula for the structure is $B_2A_{n-1}Pb_nI_{3n+1}$, where B is the replacement cation and $n$ is the number of perovskite inorganic sheets, tunable by adjusting the mixing ratio of 3D cations to 2D spacer molecules.

Adding the 2D spacer layer to 3D perovskite solar cells has been shown to offer increased protection against humidity and thermal stress[172–176]. However, these devices suffer from a reduced PCE in comparison with their 3D counterparts. After optimisation in the device preparation, state-of-the-art 2D perovskite devices now reach competitive PCEs above 14 %[177], but remain below the record 25.7 % found for 3D perovskites[159]. More recently, new devices combining a bulk 3D perovskite layer with a thin 2D layer have appeared, to benefit both from the increased stability offered by the 2D layer, and from the higher efficiency offered by the

3D layer. These 2D/3D heterostructures already reach efficiencies over 20 % (efficiencies of 21 % and 23 % were recently demonstrated[178,179]) and, most remarkably, have been shown to maintain their PCE for over a year[180–182]. While the impact of the 2D perovskite layer on external instability sources is thus established, how these 2D perovskite layers affect the ion migration dynamics in the 2D/3D heterostructures remains an open question.

Initial works on this topic of ion migration in 2D perovskites include conductivity[183,184], TOF-SIMS[43] and absorption spectroscopy measurements[185], all indicating a reduction of ion migration in the low-dimensional perovskite layers. Lin *et al.* and Xiao *et al.* showed that ion migration was completely suppressed in fully 2D perovskites - both along the out-of-plane and in-plane directions - when using n-butylammonium (BA) (with $n = 3$ or $n = 4$) as the 2D spacer molecule[183,184]. Huang *et al.* looked at TOF-SIMS signals of 3D perovskites and compared these with those of 2D perovskites with large $n$-values. They found that iodide was the dominant species migrating in the 3D devices, and that this migration was suppressed in the case of the 2D perovskites[43]. Cho *et al.* compared the speed of halide remixing as a function of $n$, and found that with lower $n$ values, the halide remixing took longer, indicating an energy barrier against ion migration for the lower-dimensionality perovskites[185]. While there seems to be an emerging consensus that 2D perovskites can either mitigate or altogether suppress the ion migration in fully 2D perovskite devices, some questions remain unanswered. These include the quantification of the effect of the 2D layer, whether a thin 2D perovskite layer has any influence on the ion migration dynamics within a stack that contains a much thicker 3D layer, and the potential impact of the 2D organic cation spacer itself.

To study these questions, we use efficient 2D/3D solar cell devices prepared with a range of 2D spacer molecules, and measure small variations induced by these thin 2D perovskite layers on top of the 3D perovskite.

## 5.2 Results and discussion

### 5.2.1 2D/3D device fabrication, with FEA, PEA and mixed FEA/PEA as 2D spacer molecules

We fabricate a range of 2D/3D perovskite stacks using either pentafluorophenethylammonium (FEA), phenethylammonium (PEA), or a mix of FEA/PEA as the 2D spacer molecule in the 2D perovskite layer. We

further complement our range of devices with a reference device containing only the 3D perovskite and no additional 2D layer. The 3D layer is a mixed-halide $MAPb(I_{0.95}Br_{0.05})_3$ perovskite. All devices have a p-i-n architecture with compact $TiO_2$ (C-$TiO_2$) and mesoporous $TiO_2$ (M-$TiO_2$) as Electron Transport Layers (ETLs) and Spiro-OMeTAD as the Hole Transport Layer (HTL). The devices are completed with Fluorine doped Tin Oxide (FTO) and gold electrodes for current extraction. An illustration is shown in Figure 5.1.

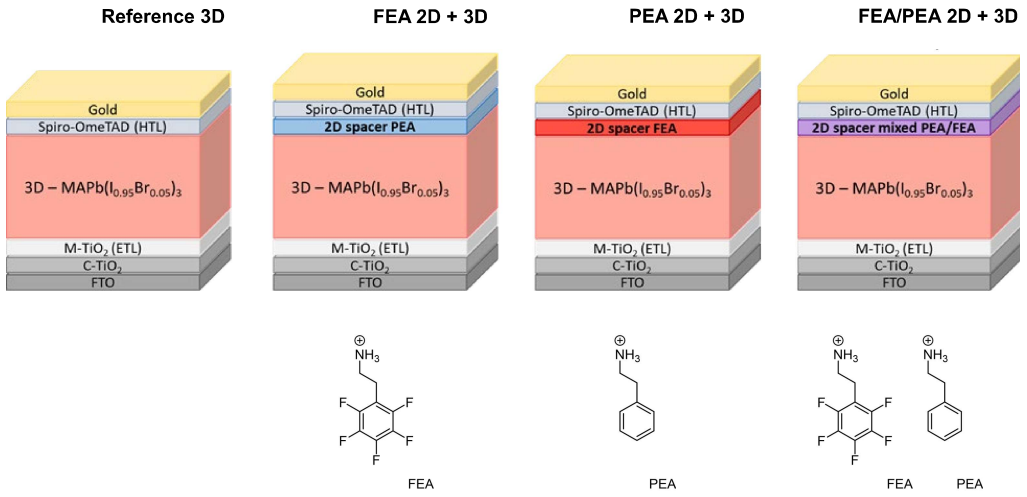


FIGURE 5.1. Solar cell device stacks, where the 3D layer is a mixed-halide $MAPb(I_{0.95}Br_{0.05})_3$ perovskite, the ETL consists of a combination of C-$TiO_2$ and M-$TiO_2$, the HTL is Spiro-OMeTAD, and the bottom and top electrodes are respectively FTO and gold. Except for the pure 3D sample, a thin 2D perovskite layer is added on top of the 3D perovskite layer, where the 2D spacer molecule is varied to obtain a range of 2D/3D stacks. The 2D spacer molecules used are FEA, PEA or a mix of FEA/PEA. The organic spacers FEA and PEA are shown below their respective stacks.

The 2D spacer molecules FEA and PEA both consist of an aromatic ring and an ammonium group, the latter allowing for coordination to the perovskite octahedra. FEA and PEA differ in the electron density distribution across the aromatic rings: fluorine atoms remove electron density from the aromatic ring in the FEA system, leading to a low electron density in the centre of the aromatic ring, whereas the electron density is highest in the centre of the aromatic ring in the PEA system. This change in the electronic distribution will modify the stacking of the 2D molecules within the 2D layer: as shown in Figure 5.2, the PEA molecules can either adopt a $\pi - \pi$ interaction with a T-shaped (t), parallel displaced

(d) or parallel (p) orientation (with interaction strengths $\pi_T \sim \pi_d < \pi_p$), while the FEA molecules will favor parallel $\pi - \pi$ interactions, $\pi_p$. In turn, this affects the strength and nature of the supramolecular interaction between the 2D and 3D perovskites[186]. Our investigation thus extends the characterisation of ion migration to 2D perovskite systems with fluorine containing spacers, in which the change in electronic density leads to a difference in the supramolecular interaction, which could affect the energy barrier for ionic motion. This variation will allow us to study whether the ion migration properties of the 2D/3D perovskite devices are impacted by the composition of the 2D spacer layer itself.

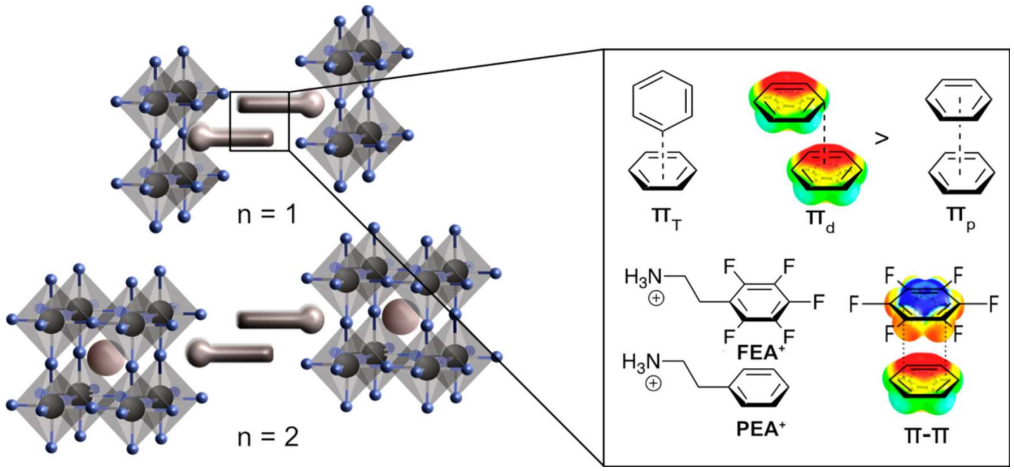


FIGURE 5.2. Illustration scheme of the possible supramolecular interactions formed within the 2D perovskite layers of either PEA or FEA. The strength of the $\pi - \pi$ interaction is dependent on the aromatic ring orientation, whether T-shaped, parallel displaced or parallel. Reproduced from reference 186.

### 5.2.2 THERMAL ADMITTANCE SPECTROSCOPY AND TRANSIENT ION DRIFT CHARACTERISATION

We measure the Thermal Admittance Spectra (TAS) of the 2D/3D perovskite devices, as shown in Figure 5.3a-d. We find that in the low-frequency regime below $10^2$ Hz, the capacitance shows very high values, from 250 to 1750 nF cm$^{-2}$, depending on the 2D spacer molecule and on the temperature. This low-frequency feature increases with temperature, indicating a thermally activated process. This feature is in line with previous works using devices with a p-i-n architecture and $TiO_2$ as the ETL[97]. It stems from an activated process in this transport layer or at the $TiO_2$/perovskite interface. The mobile ion response in per-

ovskite cells is usually also present in this frequency range[187], but this feature is expected to have lower intensity than the one observed here, especially considering that the TAS measurements are taken under dark conditions[52]. We thus assign this low-frequency peak to an effect of the $TiO_2$ layer, possibly convoluted with a mobile ion response. Since we are not interested in the effect of the $TiO_2$/perovskite interface on the capacitance, we measure at a higher frequency where this feature is absent. At higher frequencies above $10^2$ Hz, the capacitance spectra decrease to a plateau-like shape with values in the range of 50 to 150 nF cm$^{-2}$. In this frequency regime, the plateau-like spectral shape is temperature independent (see insets in Figure 5.3a-d), and the only influence of temperature is in the small shift to higher capacitance values at higher temperatures. The capacitance in this frequency regime corresponds to geometric capacitance[52], where the device is approximated as a parallel-plate capacitor. There, we assume that the small shift with temperature is linked to the previously-reported variation of the perovskite permittivity with temperature[101].

We are interested in the effect of the 2D layer on ion migration. As the mobile ion response in TAS is shadowed by the effect of the $TiO_2$ layer, we turn to Transient Ion Drift (TID) for mobile ion characterisation in these devices. There, we choose an AC frequency of $10^4$ Hz to measure the capacitance, in the intermediate frequency regime as defined above, where the capacitance corresponds to geometric capacitance. The resulting TID capacitance datasets, taken after applying a filling voltage of 1.2 V, are shown in Figure 5.3e-h. More TID capacitance datasets, taken after applying voltage pulses of 0.8 V and 1 V, are presented in Section 5.4.2. Qualitatively, the first observation is the similarity in the TID transients of the various 2D/3D perovskite devices. An initial rise in capacitance is observed in the first 10 to 20 milliseconds – this rise is mostly present at higher temperatures, above 310 K – and is followed by a decay in the following timeframe, before the capacitance transients reach their steady-state values after 100 to 200 milliseconds. This first qualitative observation is an indication for similar ion migration processes happening in the range of 2D/3D perovskite devices studied here, prepared with a 2D layer made by using FEA, PEA or a mix of FEA and PEA as the 2D spacer molecule and in the 3D devices. In the 2D/3D devices, the 2D perovskite layer is thin compared to the bulk 3D layer, so this similarity might be expected as most of the ion migration happens through the bulk. On the other hand, the TID transients, if similar, also clearly show some differences, with an evolution of the temperature at

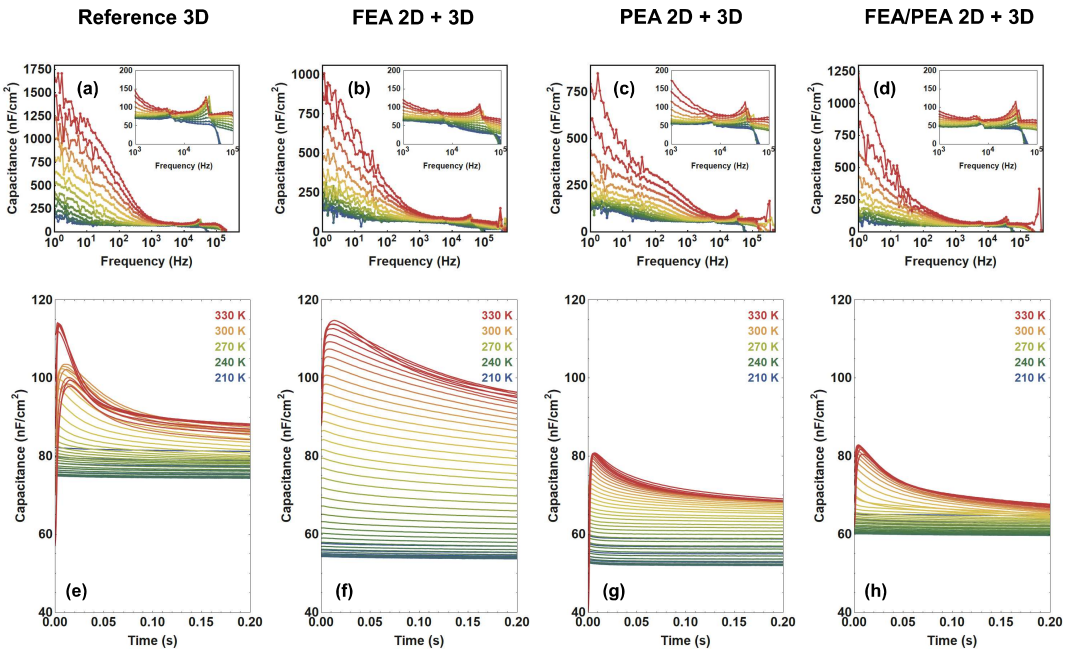


FIGURE 5.3. Admittance spectra of the 2D/3D perovskite solar cell devices, with (a) no 2D layer, (b) the 2D layer with FEA, (c) the 2D layer with PEA and (d) the 2D layer with a mix of FEA and PEA. The admittance spectra were taken at 300 K in the dark, using an AC voltage of 10 mV. TID capacitance transients of the 2D/3D perovskite solar cell devices, with (e) no 2D layer, (f) the 2D layer with FEA, (g) the 2D layer with PEA and (h) the 2D layer with a mix of FEA and PEA. The capacitance transients are taken after applying a voltage pulse of 1.2 V for 2 s and are measured at 10 kHz with an AC voltage of 10 mV. The capacitance traces are taken from 210 K to 330 K, and shown here in temperature steps of 30 K.

which the ion migration process is first observed, but also an evolution in the specific time dynamics for each of the 2D/3D perovskite systems. To further study the mobile ion dynamics in the 2D/3D systems and obtain a quantitative picture, we analyse the transients and fit them to an analytical model. The fitting procedure is detailed in the next paragraph.

### 5.2.3 QUANTIFICATION OF THE ION MIGRATION CHARACTERISTICS

The TID transients are fitted to Equation 5.1, where $C(t,T)$ is the capacitance at time $t$ and temperature $T$, $C_\infty(T)$ is the steady-state capacitance at temperature $T$, $\Delta C_n(T)$ is the amplitude of the process $n$ in the transient of temperature $T$, $p_{fit(n)}$ is a fitting parameter associated

to process $n$ and used to calculate the diffusion coefficient in later stages, and $E_{a(n)}$ is the activation energy of ion migration in process $n$.

$$C(t,T) = C_{\infty}(T) + \sum_{n} \Delta C_n(T) \exp\left(\frac{-t}{p_{fit(n)}\, T\, \exp\left(\frac{E_{a(n)}}{k_B T}\right)}\right) \tag{5.1}$$

We fit the full set of transients (measured at different temperatures) from one TID dataset in a single global fit. This allows us to determine the global values for both $p_{fit(n)}$ and $E_{a(n)}$ for each of the $n$ processes taking place, and to determine the list of $\Delta C_n(T)$ values at each temperature. To increase the fitting speed, we use a differential evolution algorithm: candidate solutions are proposed and iteratively improved based on a genetic process. In other words, "parent" solutions are combined to find the next generation of improved solutions, labelled "daughter" solutions. Such algorithms are efficient at finding global minima of the cost function in large and complex parameter spaces[188]. Further details are provided in Section 5.4.3.

The fitting procedure requires 3 exponential contributions to accurately describe the datasets, where one of the contributions describes a capacitance rise, and the two other contributions correspond to the decay dynamics.

We first consider the rise feature. This contribution is present mostly at higher temperatures and it is dependent on the applied voltage pulse (see Figures 5.5 and 5.6 in Section 5.4). At lower filling voltages, this rise starts with very low initial capacitance values at early times, below $40\,\mathrm{nF\,cm^{-2}}$ in the extreme cases. Negative capacitance and capacitance close to zero have been observed in impedance measurements with $TiO_2$/perovskite devices in the low-frequency regime[189] and are often attributed to a surface-ionic interaction. We believe that a similar mechanism upon the (seconds-long) voltage pulse leads to the initial low capacitance. When we take this feature into account for the fitting algorithm, it requires very large $\Delta C_n(T)$ values for the rise process. The TID model, however, assumes a small concentration of ions (compared to the background charge density), and hence the fitted values are above the assumption made in our model (see Section 1.6). For these reasons we exclude the rise feature from the analysis. Drift-diffusion modelling of the system could prove beneficial in the attribution of this rise event

to either an interfacial effect, or an electronic process in the perovskite layer.

The two decay features are present at all temperatures and in a reliable manner for each of the filling voltages applied (see Figure 5.3 in Section 5.2.2, and Figures 5.5 and 5.6 in Section 5.4.2), we thus attribute them to ion migration processes in the 2D/3D perovskite heterostructure devices. If we assume that the perovskite is p-type[122,190,191], then a decay in TID capacitance corresponds to migration from an anion species. In the case of lead halide perovskites, this capacitance decay is thus attributed to migration from the halide species. This result matches well with literature, as the halide ion is often found to be the most mobile ion species in perovskite solar cells[43,56,108].

### 5.2.4 Halide migration in the 2D/3D perovskites

We now look at the quantified picture of halide migration in the fabricated solar cell devices and study the influence of the thin 2D layer on the ion dynamics in the full 2D/3D perovskite system, comparing the reference device prepared with only the 3D perovskite, and the 2D/3D perovskites made using either FEA, PEA or a mix of these two as the 2D spacer molecule. We find that in all systems incorporating a 2D layer, the halide migration process is hindered compared to the pure 3D case. The nature of this reduction in ion migration is, however, dependent on the composition of the 2D perovskite. The values plotted in Figure 5.4 are also reproduced in Table I for clarity.

The device including FEA for the 2D thin layer acts as a barrier for halide ion migration by reducing the mobile ion density of one of the mobile species, which we call Halide (1), shown in orange in Figure 5.4b. Specifically, the mobile ion density decreases from 41 % to 15 % of the doping density.

The device including PEA for the 2D thin layer also acts as a barrier for halide ion migration, but the mechanism is different. There, on top of the reduction in mobile ion density - from $\sim$ 60 % to 25 % of the doping density, there is also a significant increase in the activation energy for the migration step of Halide (2), from $\sim$ 65 meV without PEA to 110 meV after addition of PEA as the 2D spacer molecule. Interestingly, both activation energy and density of Halide (2) are affected by PEA, compared to the system with FEA which affects the Halide (1) process only.

We also study the effect of mixing both FEA and PEA as spacer

molecules in the thin 2D layer. This mixture leads to supramolecular interaction which should strengthen the interaction within the 2D spacer layer[173,192–194]. There, similar to the case with PEA only, we observe both an increase in the activation energy of Halide (2), and a decrease in the density of mobile Halide (2) ion. The values are comparable when using either only PEA or the mix of PEA and FEA: the activation energy remains 110 meV, and the mobile ion density arrives at $(25 \pm 5)$ % and $(28 \pm 13)$ % of the doping density. In other words, the ion migration effect observed when using the mixed FEA/PEA system is dominated by the ion migration response of PEA.

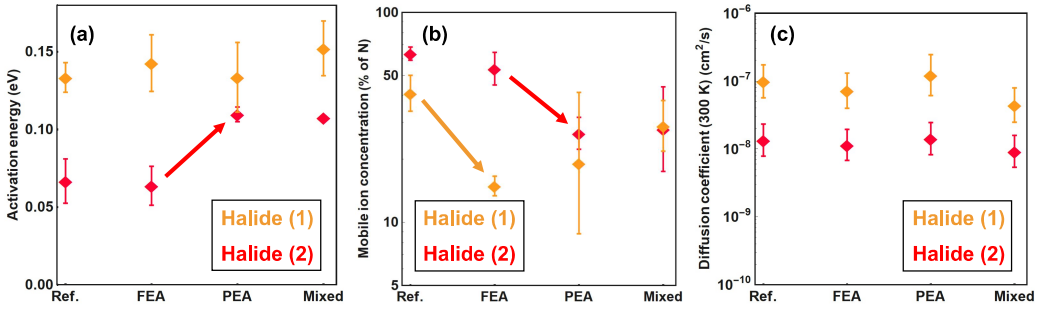


FIGURE 5.4. Ion migration characteristics of the 2D/3D perovskite solar cell devices prepared either with no 2D layer, or FEA, PEA or a mix of FEA and PEA as 2D spacer molecule in the 2D perovskite layer; with (a) the activation energies for the migration step, (b) the density of mobile ions, and (c) the diffusion coefficient of these mobile ions. The 2 different mobile halide species are shown in orange and in red.

The feature that remains constant between the fully 3D perovskite system and all of the 2D/3D perovskite systems studied here is the ion diffusion coefficients of mobile ion species Halide (1) and Halide (2). To test whether these values can indeed be considered constant, we use an unpaired student's t-test, and find that there is no statistically significant trend as a function of the 2D spacer layer. The diffusion coefficient of Halide (1) is on the order of $10^{-7}\,\mathrm{cm^2 s^{-1}}$, and that of Halide (2) on the order of $10^{-8}\,\mathrm{cm^2 s^{-1}}$. Both diffusion coefficients are in line with previous works on the halide diffusion coefficient in perovskite solar cells[56,76,124].

The migration activation energies in the fully 3D reference system are very close to those previously found for the mixed-halide perovskite of similar composition, $MAPbBr_{0.3}I_{2.7}$ (see Chapter 3, Section 3.2.3)[104]. This 3D perovskite with 10 % bromide addition showed two mobile halide species with activation energies of 0.060 eV and 0.150 eV[104], comparable

| | Pure 3D | FEA 2D + 3D | PEA 2D + 3D | FEA/PEA 2D + 3D |
|---|---|---|---|---|
| | | | | |
| $E_a$ Halide (1) (eV) | $0.134 \pm 0.010$ | $0.143 \pm 0.018$ | $0.134 \pm 0.022$ | $0.152 \pm 0.018$ |
| $E_a$ Halide (2) (eV) | $0.067 \pm 0.014$ | $0.064 \pm 0.013$ | $0.110 \pm 0.005$ | $0.108 \pm 0.001$ |
| | | | | |
| Density Halide (1) (% of $N_D$) | $41 \pm 8$ | $15 \pm 1.6$ | $19 \pm 15$ | $29 \pm 8$ |
| Density Halide (2) (% of $N_D$) | $64 \pm 5$ | $54 \pm 10$ | $25 \pm 5$ | $28 \pm 13$ |
| | | | | |
| D Halide (1) ($\mathrm{cm^2\,s^{-1}}$) | $(1.0 \pm 0.6) \times 10^{-7}$ | $(7.0 \pm 4.0) \times 10^{-8}$ | $(1.2 \pm 0.9) \times 10^{-7}$ | $(4.4 \pm 2.6) \times 10^{-8}$ |
| D Halide (2) ($\mathrm{cm^2\,s^{-1}}$) | $(1.3 \pm 0.7) \times 10^{-8}$ | $(1.1 \pm 0.6) \times 10^{-8}$ | $(1.4 \pm 0.8) \times 10^{-8}$ | $(9.0 \pm 5.0) \times 10^{-9}$ |

Table I. Extracted parameters for the activation energies, the mobile ion densities, and the diffusion coefficients of the mobile ion species (1) and (2) as measured by TID spectroscopy in the 2D/3D perovskite solar cell devices.

to the 0.067 eV and 0.134 eV found here, suggesting similar migration pathways in both of these mixed-halide 3D perovskites. When comparing the mobile ion densities of Halide (1) and Halide (2) in the fully 3D reference system, we find that they are both on the same order of magnitude, with $(41 \pm 8)$ % of the doping density for Halide (1), and $(65 \pm 5)$ % for Halide (2). The bromide concentration in the 3D perovskite represents only 5 % of the iodide concentration: if the two different mobile ions Halide (1) and Halide (2) were iodide and bromide, we would expect a clear difference in the density of mobile ions. The similarity in mobile ion density thus suggests that both contributions stem from the prominent halide in the $MAPb(I_{0.95}Br_{0.05})_3$ perovskite, i.e. the iodide species. This is in line with previous work showing iodide to be a more mobile ion than bromide[68,73,116]. We thus attribute the two migration processes Halide

(1) and Halide (2) to iodide migration. Determining the specific nature of the two different migration processes would facilitate the development of strategies to manage ion migration, and thus calls for future investigation. We also note the large uncertainty in the determination of the halide density. This is partially due to a large sample-to-sample variation, and partially because at such high density (compared to the doping density) the ions are not forming a mere perturbation to the electric field distribution inside the device. Hence, the simple theory we use for the analysis is not entirely accurate, limiting the accuracy with which we can determine the ion density. Ongoing work on simulating the full electric field distribution in the device could shed light on these uncertainties.

Together, our results thus show a prominent effect of the thin 2D layer addition on top of the thicker 3D perovskite in terms of ion migration reduction. To observe such a large effect might be surprising, considering the difference in thickness between these two layers. One explanation might come from the role of the transport layers in the perovskite device stacks. In our general model of lead halide perovskite devices, we assume that these transport layers are fully ion-blocking, meaning that the mobile ions only drift through the perovskite layer and to the interface between perovskite and transport layer. If, however, there is some transfer of the mobile ions into the transport layers, in other words if this hypothesis is invalid in the fully 3D case, then the impact of a completely ion-blocking layer, however thick, at the interface with this 3D perovskite would be consequential. We thus consider the 2D perovskite layer to have better ion-blocking properties than the usual electron and hole transport layers.

## 5.3 Conclusion

We study the influence of the addition of a thin 2D perovskite layer on top of a bulk 3D perovskite layer, in terms of ion migration in the full 2D/3D solar cell device, and further evaluate the effect of the 2D perovskite composition by varying the 2D spacer molecules with FEA, PEA or a mix of FEA and PEA. We find that in all systems incorporating a 2D perovskite layer, the 2D/3D solar cell device shows a reduction in halide migration. The mechanism however differs, with either a reduction in the mobile density of Halide (1) for the pure-FEA case, or a combination of a reduction in the mobile density and an increase in the activation energy of Halide (2) for the pure-PEA case and the mixed FEA and PEA

case. These results highlight the crucial role played by 2D perovskites in hindering ion diffusion through the stack of efficient solar cell devices, while suggesting the presence of different mechanisms of blocking ion migration for different 2D spacers. Detailed understanding of the impact of the 2D spacer on ion migration processes might finally pave the way towards perovskite photovoltaics with long term stability.

## 5.4 Appendix

### 5.4.1 Device fabrication

The devices are fabricated according to previously published procedures[173,186,193]. The thickness of the 3D perovskite layer was shown to vary between 400 and 500 nm.

### 5.4.2 Electrical measurements

All electrical measurements are taken in the dark, using a commercially available setup from Semetrol and a JANIS VPF-100 cryostat. To avoid oxygen or moisture contamination, the pressure is kept below $7 \times 10^{-6}$ mbar during the measurements and the loading of the samples into the cryostat takes place in a nitrogen-filled glovebox.

TAS spectra are recorded from 1 Hz to 500 kHz in 100 steps, using a 10 mV perturbation voltage. The measurement is repeated every 10 K, from 210 K up to 340 K. We measure TID after applying a voltage pulse for 2 seconds and record the capacitance transients between 210 and 330 K, with temperature steps of 3 K. The different filling voltages applied are 0.8, 1.0 and 1.2 V, and the AC perturbation voltage used to measure capacitance is 10 mV applied with a frequency of 10 kHz. For each temperature transient, 2033 data points are collected (i.e. $\sim$ 1 s after $t = 0$), and the capacitance transients are averaged over 20 repetitions before moving to the next transient. All TAS and TID measurements are repeated on 2 different cells, coming from separate batches prepared by using the same recipe (i.e. two pure 3D cells and six 2D/3D systems, with 2×FEA, 2×PEA and 2×mixed FEA/PEA).

The TID technique, as well as the analytical model and hypotheses used, are described in Chapter 1 of this thesis.

In Figures 5.5 and 5.6, we show the TID datasets after applying filling voltages of 0.8 V and 1 V, for the 4 different types of solar cell devices prepared - the pure 3D device, and the set of 2D/3D heterostructure devices with FEA, PEA and the mixture of FEA and PEA as 2D spacer molecules. In Figure 5.5, which represents the case after applying a voltage of 0.8 V, we notice that the transients are visible, but have a much lower magnitude than in the cases with filling voltages of 1 V or 1.2 V (shown in Figure 5.6 and Figure 5.3, respectively). We conclude that 0.8 V is not sufficient to fully collapse the depletion in the devices. In Figure 5.6 however, which represents the case after applying a voltage of 1 V, we notice that the dynamics in the capacitance transients are very

similar to those observed after applying a voltage of 1.2 V, with an initial rise in the first 10 to 20 ms before a decay in the following 100 ms, and finally a saturation after $\sim$ 150 ms. This indicates that the 1 V filling voltage is sufficient for the devices to be almost or fully depleted, and that the ion migration dynamics taking place are equivalent to those observed after application of the 1.2 V filling bias. To obtain a reliable quantification of the ion migration dynamics in the 2D/3D perovskite systems, we thus decide to use the TID datasets measured at 1 V and 1.2 V.

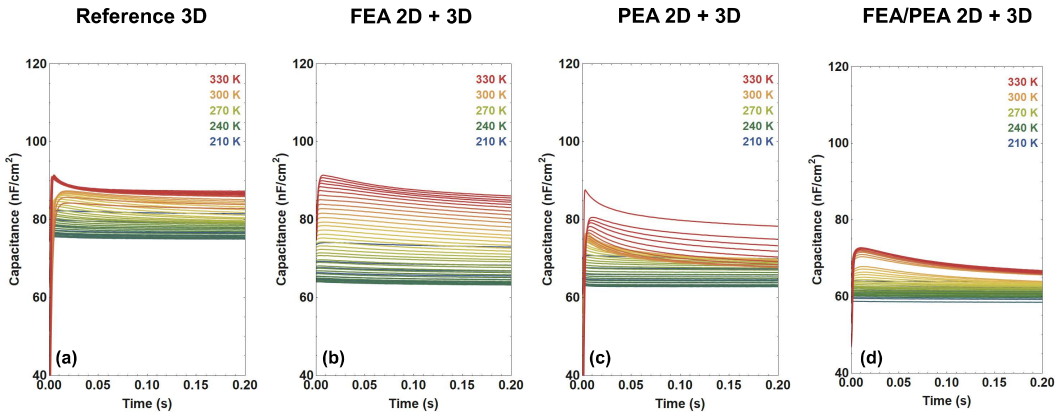


FIGURE 5.5. TID capacitance transients of the 2D/3D perovskite solar cell devices taken after applying a voltage pulse of 0.8 V for 2 s, for the devices with (a) no 2D layer, (b) the 2D layer with FEA, (c) the 2D layer with PEA and (d) the 2D layer with a mix of FEA and PEA. The capacitance transients are measured at 10 kHz with an AC voltage of 10 mV. The capacitance traces are taken from 210 K to 330 K, with temperature steps of 3 K.

The feature which evolves the most between the 0.8 and 1 V TID datasets compared to the 1.2 V TID dataset is the magnitude of the initial rise event, where the peak shows larger magnitude in the 2 cases with lower voltage pulses. This observation further strengthens our analysis of this rise event being caused by either an interface effect or an electronic process rather than an ion migration process.

### 5.4.3 FITTING PROCEDURE

To obtain the values shown in Figure 5.4 and in Table I, we fit the TID datasets to Equation 5.1 (shown in Section 5.2.3). For each composition, the extracted value is taken from averaging over two filling voltages (the TID datasets obtained after applying the 1 V and 1.2 V filling voltages)

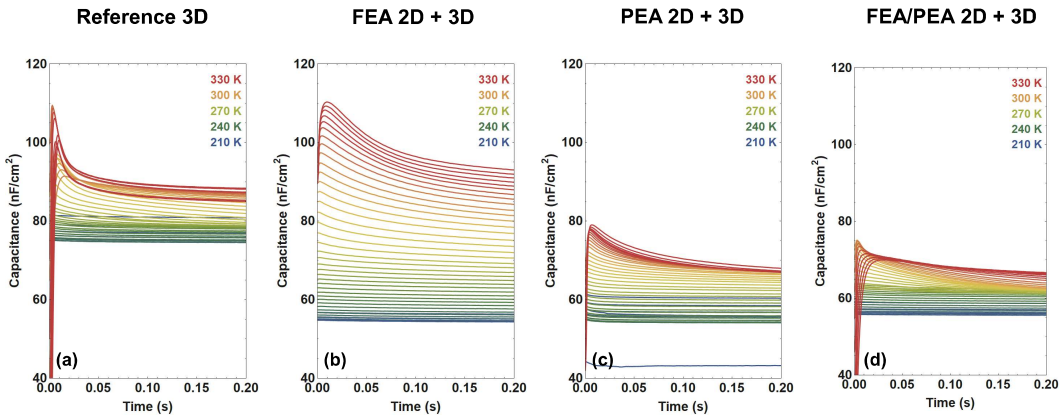


FIGURE 5.6. TID capacitance transients of the 2D/3D perovskite solar cell devices taken after applying a voltage pulse of 1 V for 2 s, for the devices with (a) no 2D layer, (b) the 2D layer with FEA, (c) the 2D layer with PEA and (d) the 2D layer with a mix of FEA and PEA. The capacitance transients are measured at 10 kHz with an AC voltage of 10 mV. The capacitance traces are taken from 210 K to 330 K, with temperature steps of 3 K.

and two device copies for each of the device compositions (2×pure 3D, 2×FEA, 2×PEA and 2×mixed FEA/PEA). The resulting averages are thus taken over a set of 4 measurements and the error bars represent the standard deviation of the mean over these measurements. The reasoning for averaging over two filling voltages is explained in Section 5.4.2 above.

The fitting procedure is based on a differential evolution algorithm, here using scipy's differential evolution function[195]. In such differential evolution algorithms, the genetic selection of "daughter" solutions is stochastic in nature. To counteract this effect, the fitting process is repeated at least 10 times for each dataset, which allows us to acquire sufficient statistics on the obtained parameters. The solutions are then filtered based on their cost function[196], which is a measure of how well the fitted function matches the datasets. These are obtained by taking the sum of the residuals squared for each temperature trace and summing them together in a dataset-wide cost value. Finally, the fitted parameters of the remaining solutions are averaged – the resulting values are reported in Table I.

To avoid the cost function being dominated by the traces with the highest decay amplitudes (i.e. the traces at highest temperatures), we normalize all temperature traces prior to the fitting procedure.

The differential evolution algorithm has tunable parameters to optimise a quick route to a reliable global fit. To increase the likelihood

| | |
|---|---|
| $\Delta C_n(T)$ (pF) | $-30$ to 2 |
| $p_{fit(n)}$ ($\mathrm{s\,K^{-1}}$) | $10^{-8}$ to $10^{-4}$ |
| $E_{a(n)}$ (eV) | 0.01 to 0.3 |
| $C_\infty(T)$ (pF) | $10^{-6}$ to 0.5 |
| Tolerance factor | 0.002 to 0.1 |
| Mutation factor | 0.4 to 0.6 |
| Cost treshold | 6 to 33 |

Table II. Set of parameters and the range of values used for the fitting procedure.

of finding the global minimum, either more iterations, a higher mutation factor or a lower tolerance factor can be set, all at the expense of computational power. To avoid any prior bias on the results, a broad parameter range was applied throughout the entire fitting process. The typical parameter ranges used are shown in Table II.

The maximum value of the activation energy for ion migration chosen here is on the low end compared to some of the previously reported values[86,131,148]. This range was chosen due to the observation that using higher activation energies in the initial parameter set did not result in better convergence of the extracted value. Indeed, allowing the activation energies to increase up to 1.2 V resulted in similar final values, far below 0.3 V, while the larger parameter space required significantly more computational power.